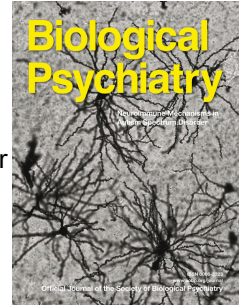


# Journal Pre-proof



Midbrain dopamine controls anxiety-like behavior by engaging unique interpeduncular nucleus microcircuitry

Steven R. DeGroot, Rubing Zhao-Shea, Leeyup Chung, Paul M. Klenowski, Fangmiao Sun, Susanna Molas, Paul D. Gardner, Yulong Li, Andrew R. Tapper

PII: S0006-3223(20)31707-8

DOI: <https://doi.org/10.1016/j.biopsych.2020.06.018>

Reference: BPS 14260

To appear in: *Biological Psychiatry*

Received Date: 3 March 2020

Revised Date: 15 June 2020

Accepted Date: 16 June 2020

Please cite this article as: DeGroot S.R., Zhao-Shea R., Chung L., Klenowski P.M., Sun F., Molas S., Gardner P.D., Li Y. & Tapper A.R., Midbrain dopamine controls anxiety-like behavior by engaging unique interpeduncular nucleus microcircuitry, *Biological Psychiatry* (2020), doi: <https://doi.org/10.1016/j.biopsych.2020.06.018>.

This is a PDF file of an article that has undergone enhancements after acceptance, such as the addition of a cover page and metadata, and formatting for readability, but it is not yet the definitive version of record. This version will undergo additional copyediting, typesetting and review before it is published in its final form, but we are providing this version to give early visibility of the article. Please note that, during the production process, errors may be discovered which could affect the content, and all legal disclaimers that apply to the journal pertain.

© 2020 Published by Elsevier Inc on behalf of Society of Biological Psychiatry.

1  
2  
3  
4  
5  
6  
7  
8  
9  
10  
11  
12  
13  
14  
15  
16  
17  
18  
19

**Midbrain dopamine controls anxiety-like behavior by engaging unique  
interpeduncular nucleus microcircuitry**

**Authors**

Steven R. DeGroot<sup>1,2</sup>, Rubing Zhao-Shea<sup>1</sup>, Leeyup Chung<sup>1</sup>, Paul M. Klenowski<sup>1</sup>,  
Fangmiao Sun<sup>3,4</sup>, Susanna Molas<sup>1</sup>, Paul D. Gardner<sup>1</sup>, Yulong Li<sup>3,4,5</sup>, Andrew R. Tapper<sup>1\*</sup>

<sup>1</sup>Brudnick Neuropsychiatric Research Institute, Dept. of Neurobiology, University of  
Massachusetts Medical School, Worcester, MA, 01605, USA

<sup>2</sup>Graduate Program in Neuroscience, University of Massachusetts Medical School,  
Worcester, MA, 01605, USA

<sup>3</sup>State Key Laboratory of Membrane Biology, Peking University School of Life Sciences,  
100871 Beijing, China

<sup>4</sup>PKU-IDG/McGovern Institute for Brain Research, 100871 Beijing, China

<sup>5</sup>Peking-Tsinghua Center for Life Sciences, 100871 Beijing, China

\*Lead Contact, Correspondence to: [andrew.tapper@umassmed.edu](mailto:andrew.tapper@umassmed.edu)

Short Title: VTA dopamine modulates IPN activity to control anxiety

## 20 Background

21 Dopamine (DA) is hypothesized to modulate anxiety-like behavior although the precise  
22 role of DA in anxiety behaviors and the complete anxiety network in the brain have yet  
23 to be elucidated. Recent data indicate dopaminergic projections from the ventral  
24 tegmental area (VTA) innervates the interpeduncular nucleus (IPN), but how the IPN  
25 responds to dopamine (DA) and what role this circuit plays in anxiety-like behavior is  
26 unknown.

## 27 Methods

28 We expressed a genetically encoded GPCR-activation-based-DA sensor in mouse  
29 midbrain to detect DA in IPN slices using fluorescence imaging combined with  
30 pharmacology. Next, we selectively inhibited or activated VTA→IPN DAergic inputs via  
31 optogenetics during anxiety-like behavior. We utilized a biophysical approach to  
32 characterize DA effects on neural IPN circuits. Site-directed pharmacology was used to  
33 test if DA receptors in the IPN can regulate anxiety-like behavior.

## 34 Results

35 DA was detected in mouse IPN slices. Silencing/activating VTA→IPN DAergic inputs  
36 oppositely modulated anxiety-like behavior. Two neuronal populations in the ventral IPN  
37 (vIPN) responded to DA via D1 receptors (D1R). vIPN neurons were controlled by a  
38 small population of D1R neurons in the caudal IPN (cIPN) that directly respond to VTA  
39 DAergic terminal stimulation and innervate the vIPN. IPN infusion of a D1R agonist and  
40 antagonist bidirectionally controlled anxiety-like behavior.

41 Conclusions

42 VTA DA engages D1R-expressing neurons in the cIPN that innervate vIPN thereby  
43 amplifying the VTA DA signal to modulate anxiety-like behavior. These data identify a  
44 DAergic circuit that mediates anxiety-like behavior through unique IPN microcircuitry.

45 **Keywords**

46 Anxiety, Circuitry, Dopamine, Interpeduncular Nucleus, Ventral Tegmental Area, Medial  
47 Habenula

48

49

50

51

52

53

54

55

56

57

58

59

**60 Introduction**

61 Anxiety is a complex, multi-circuit behavioral phenomenon characterized by a prolonged  
62 sense of unease and heightened arousal in the absence of a direct threat(1). Persistent  
63 uncontrolled anxiety inappropriate to the level of threat underlies anxiety disorders  
64 which are often comorbid with depression and many other psychiatric disorders(2).  
65 Understanding the neurocircuitry that regulates anxiety is necessary to inform future  
66 anxiolytic therapy development.

67 Basal and stress-induced anxiety states are governed by brain regions that process  
68 emotions including prefrontal cortex (PFC), hippocampus, and extended amygdala(3).  
69 Each of these regions is regulated by modulatory input from dopamine (DA)-rich  
70 midbrain areas that are hypothesized to shape anxiety-like behavior(4,5,6,7), although  
71 the exact role of DA and how it drives behavior in response to anxiogenic stimuli are  
72 unknown. Emerging data implicate a much more understudied pathway that contributes  
73 to fear and anxiety-like behavior, the habenulo-interpeduncular axis(8,9,10,11). This  
74 pathway consists of neurons in the medial habenula (mHb) that project to the  
75 interpeduncular nucleus (IPN)(12). While the mHb receives input from the septum, the  
76 IPN transmits forebrain input to the mid- and hindbrain resulting in the regulation of  
77 behavior(13,14). The majority of studies on the mHb→IPN circuit have focused on  
78 nicotine addiction-associated behaviors, where this pathway has been implicated in  
79 regulating drug intake and aversive, affective, as well as physical aspects of nicotine

80 withdrawal(15,16,17,18,19). The habenulo-interpeduncular pathway also contributes to  
81 regulating baseline anxiety-like behavior(20,21), although the mechanism(s) involved,  
82 particularly in the IPN, are not clearly understood.

83 We recently described a mesointerpeduncular circuit in which VTA DAergic neurons  
84 project to the neighboring IPN(22). While the DAergic neuron-rich VTA is largely  
85 associated with increased motivation towards novelty, reinforcement, and positive  
86 affective state, the IPN is a brain region governing reduced motivation towards  
87 familiarity, as well as aversion, and negative affective state(19,22,23,24,25,26,27).  
88 Thus, general activity in these two regions promotes opposing behaviors suggesting the  
89 mesointerpeduncular circuit could act as an important balancing point governing  
90 motivation and anxiety-like behavior. Indeed, previously we showed that stimulating this  
91 pathway with optogenetic tools could shift the motivational aspects of familiar stimuli  
92 interactions and enhance their salience as if they were novel(22). Here, we provide a  
93 comprehensive understanding on the mechanistic connection between the VTA and IPN  
94 and how endogenous DA released from this circuitry contributes to anxiety-associated  
95 behaviors.

## 96 **Materials and Methods**

### 97 **Animals**

98 All experiments followed the guidelines for care and use of laboratory animals provided  
99 by the National Research Council, and with approved animal protocols from the  
100 Institutional Animal Care and Use Committee of the University of Massachusetts  
101 Medical School. C57Bl/6J (#000664), GAD2-Cre (#010802), Chat-Cre (#006410), DAT-

102 Cre (#006660), Chat-ChR2 (#014546), DRD1-Cre (#028298), and *Drd1a*-tdTomato  
103 (#016204) mice were obtained from The Jackson Laboratory, bred in the UMMS animal  
104 facility and used in behavioral, optogenetic and biophysical experiments as indicated.  
105 Cre lines were crossed with C57Bl/6J mice and only heterozygous animals carrying one  
106 copy of the Cre recombinase gene were used for experimental purposes. Mice were  
107 housed together in cages of no more than five animals and kept on a standard 12 h  
108 light/dark cycle (lights ON at 7 A.M.) with ad libitum access to food and water. Three to  
109 four weeks before experimentation, subject mice were kept under a reverse 12 h  
110 light/dark cycle (lights ON at 7 P. M.) for at least 5 days before any behavioral testing

### 111 **Viral Preparation**

112 Optogenetic plasmids were packaged into AAV serotype 2 (AAV2) viral particles by the  
113 UMMS Viral Vector Core. GRAB<sub>DA2m</sub> is derived from GRAB<sub>DA1m</sub>, with additional  
114 mutations in cpEGFP. GRAB<sub>DA2m</sub> has ~3-fold improvement in the maximal  $\Delta F/F_0$  and  
115 similar apparent affinity ( $EC_{50}$ ~90 nM). Detailed characterizaion of GRAB<sub>DA2m</sub> will be  
116 published elsewhere. GRAB<sub>DA2m</sub> was packaged into AAV9 by Vigene Biosciences.  
117 Additional Materials and Methods can be found in Supplementary Materials.

### 118 **Results**

#### 119 **DA is released in the IPN.**

120 To test if endogenous DA release in the IPN occurs and may be involved in anxiety-like  
121 behavior, we expressed an enhanced genetically encoded GPCR-activated DA sensor  
122 (GRAB<sub>DA2m</sub>, see Methods) that changes in fluorescence upon DA binding, in the IPN of

123 C57Bl/6J mice using AAV-mediated gene delivery(28). To test appropriate function of  
124 GRAB<sub>DA2m</sub>, we prepared midbrain slices and measured changes in fluorescence in the  
125 IPN during bath application of neurotransmitter (Figure 1A). As expected, we recorded  
126 robust increase in fluorescence intensity in response to 10 and 100  $\mu$ M DA, with a  
127 lesser response to norepinephrine (NE) and no significant response to ACh, GABA, or  
128 glutamate (Figure 1A). To test if endogenous DA could be detected in IPN slices, we  
129 measured changes in fluorescence in response to the monoamine transporter  
130 substrate, amphetamine (Figure 1B). Bath application of amphetamine increased signal  
131 of GRAB<sub>DA2m</sub>, which was significantly blocked by preapplication of the D2 receptor  
132 antagonist, haloperidol indicating that the amphetamine-induced signal was mediated  
133 by GRAB<sub>DA2m</sub>. In addition, the amphetamine-induced signal persisted in the presence  
134 of the norepinephrine transporter inhibitor, desipramine, confirming that the signal was  
135 mediated by endogenous IPN DA release as opposed to NE (Figure 1C).

136 Together, these data indicate that endogenous DA is released in the IPN, a  
137 phenomenon which may be critical for regulating anxiety-like behavior.

### 138 **DA VTA afferents in the IPN bidirectionally modulate anxiety-like behaviors.**

139 A subpopulation of DAergic neurons in the VTA project to the IPN constituting a  
140 mesointerpeduncular pathway(18,22). To test if VTA→IPN axon terminals are the  
141 source of DA release and contribute to anxiety-like behaviors, we selectively expressed  
142 Cre-dependent halorhodopsin (NpHR)-eYFP in the VTA of DA transporter (DAT)::Cre  
143 mice via AAV2-mediated gene delivery and implanted fiber optic cannulas into the IPN  
144 to deliver yellow light (593nm, constant light, 20s on, 10s off, Figure 2A, S2) and photo-

145 inhibit VTA<sup>DA</sup>→IPN inputs during the elevated plus maze (EPM)(29, 30). VTA<sup>DA</sup>→IPN  
146 photo-inhibition resulted in a decrease in open arm time in the EPM compared to light-  
147 on eYFP controls (Figure 2B). VTA<sup>DA</sup>→IPN photo-inhibition had little effect on total arm  
148 entries compared to control conditions, suggesting normal locomotion in these animals.  
149 We also evaluated VTA<sup>DA</sup>→IPN photo-inhibition in the open field test (OFT) and  
150 observed a decrease in center time and no effect of photoinhibition on total activity  
151 (Figure 2C). To test the effect of activating VTA<sup>DA</sup>→IPN on open arm exploration, we  
152 selectively expressed Cre-dependent channelrhodopsin (ChR2)-eYFP in the VTA of  
153 DAT::Cre mice via AAV2-mediated gene delivery (Figure 2D, S1)(23). A fiber optic  
154 cannula was implanted targeting the IPN for blue-light stimulation of VTA<sup>DA</sup>→IPN inputs  
155 (473nm, 15 Hz, 20 ms/pulse, 5 s light-on, 5 s light off) during behavioral testing in the  
156 EPM. Photostimulation of VTA<sup>DA</sup>→IPN inputs significantly increased time spent in the  
157 open arms of the EPM compared to control mice expressing eYFP and receiving light  
158 stimulation, while having little effect on total arm entries compared to control conditions  
159 (Figure 2E). In the OFT, photostimulation of VTA<sup>DA</sup>→IPN increased time spent in the  
160 center compared to controls without significantly affecting total distance traveled (Figure  
161 2F). To test if behavioral results obtained with our optogenetic approach could be due to  
162 silencing/activating of VTA DAergic neurons directly, we placed fiber optic cannulas  
163 dorsal to the IPN, targeting the VTA (Figure S2). Silencing VTA neurons increased  
164 open arm time in the EPM compared to eYFP controls (Figure S3A), an effect opposite  
165 to specific VTA<sup>DA</sup>→IPN inhibition, but did not significantly impact behavior in the OFT  
166 (Figure S3C); whereas activating VTA neurons with ChR2 did not significantly change  
167 open arm time in the EPM compared to eYFP controls (Figure S3B), but significantly

168 decreased center time in the OFT. Together, these data indicate that the VTA<sup>DA</sup>→IPN  
169 pathway is a critical component of anxiety circuitry that, when engaged, drives reduced  
170 anxiety-like behavior.

171 **Two neuronal populations in the ventral IPN differentially respond to DA via D1-**  
172 **like, but not D2-like, DA receptors.**

173 To determine DA responses in IPN neurons, we used electrophysiology in acute coronal  
174 slices of C57Bl/6J mice. In cell-attached mode, we measured spontaneous action  
175 potentials (spAPs) during a five-minute bath application of exogenous 10  $\mu$ M DA (Figure  
176 3). In the ventral IPN (vIPN), 18 out of 39 neurons responded to DA with an increase in  
177 spontaneous action potential (spAP) frequency that reversed upon washout (designated  
178 as “Type A” neurons, Figure 3A, B, C), while 17 out of 39 neurons responded to DA with  
179 a decrease in spAP frequency that reversed upon washout (designated as “Type B”  
180 neurons, Figure 3D, E, F). The remaining 4 neurons exhibited no obvious responses  
181 (Figure 3G). To examine the physiological properties and current-voltage relationship of  
182 these two types of vIPN neurons, we injected 100 pA to -100 pA current in -20 pA steps.  
183 Type A and Type B neurons exhibited clear significant differences in their response to  
184 current injection and input resistance (Figure 3H-I), with Type A neurons having a lower  
185 input resistance compared to Type B neurons.

186 To test which DA receptors are required for DA-induced changes in spAP frequency in  
187 the vIPN, DA was applied to Type A and Type B neurons in the absence and presence  
188 of the D1-like receptor antagonist, SCH39166 (10  $\mu$ M) or the D2-like receptor  
189 antagonist, eticlopride (10  $\mu$ M, Figure 4A-C). SCH39166, but not eticlopride,

190 significantly attenuated DA-mediated spAP frequency changes both in Type A and Type  
191 B neurons, suggesting that DA acts through D1-like but not D2-like DA receptors in the  
192 IPN. In addition, to further rule out D2 effects, we applied a D2-like DA receptor agonist,  
193 quinpirole, to vIPN neurons and did not observe any changes in spAP frequency,  
194 spontaneous excitatory post-synaptic current (spEPSC) frequency or amplitude (Figure  
195 S4).

#### 196 **DA modulates vIPN neurons via presynaptic DA receptors.**

197 To assess how D1-like DA receptors modulate vIPN neuron activity, we recorded from  
198 Type A and B neurons under voltage-clamp and measured changes in excitatory input.  
199 DA was bath applied and neurons were voltage-clamped at -70 mV to record spEPSCs.  
200 Of note, DA failed to induce obvious inward or outward post-synaptic currents under  
201 voltage-clamp (data not shown). However, DA increased spEPSC frequency in Type A  
202 neurons while decreasing spEPSCs frequency in Type B neurons, with no effect on the  
203 spEPSC amplitude in either neuron type, suggesting DA affects excitatory inputs via DA  
204 receptors that are presynaptic (Figure 4D-I). The valence of spEPSC frequency was  
205 also consistent with the DA-induced changes in spAP frequency observed in the two  
206 vIPN neuron sub-types. In addition, when spEPSCs were blocked by NMDA and AMPA  
207 receptor antagonists (20  $\mu$ M AP-5 and 10  $\mu$ M CNQX), the majority of vIPN neurons  
208 ceased firing, suggesting that the change in spEPSC frequency induced by DA directly  
209 causes the DA-induced change in spAP frequency (Figure S5). These findings indicate  
210 that DA increases presynaptic excitatory transmission to Type A neurons and  
211 decreases presynaptic excitatory transmission to Type B neurons.

**212 cIPN neurons respond to afferent VTA DAergic terminal stimulation**

213 To test if vIPN neurons respond to DAergic inputs from the VTA, we selectively  
214 expressed Cre-dependent ChR2-eYFP in VTA DAergic neurons of DAT::Cre mice and  
215 we recorded vIPN neuronal responses upon light-induced VTA<sup>DA</sup>→IPN stimulation  
216 (Figure 5; 20 Hz, 2 ms pulse width). VTA DAergic terminals were stimulated through the  
217 microscope objective focused on the area around the recorded IPN neuron (Figure 5A).  
218 Cell-attached mode was used to record spAPs. Interestingly, the majority of vIPN  
219 neurons failed to respond to VTA terminal optic stimulation (Figure S7A). Previously,  
220 using mice in which the fluorophore td-Tomato is under the control of the *DRD1* (the  
221 gene encoding the DA D1 receptor) promoter (the *Drd1a*-tdTomato line(31)), we  
222 determined that D1 receptor expression is localized to soma in the caudal IPN (cIPN)  
223 while presumed terminal fields are localized to the vIPN (also see Figure S6A), raising  
224 the possibility that VTA→IPN DA innervation may be sub-region (i.e. cIPN) specific. In  
225 DAT<sup>Cre</sup>::eYFP mice, we observed VTA DAergic inputs in the cIPN but not rostral IPN  
226 (Figures S6A, S6B) supporting this hypothesis. In addition, D1-TdTomato midbrain  
227 slices immuno-labeled for DAT revealed TdTomato-positive neurons in cIPN decorated  
228 with DAT-immunopositive puncta (Figure S6C). In contrast to vIPN neurons, light-  
229 evoked responses were observed in the cIPN matching the VTA→IPN innervation  
230 pattern. As compared to vIPN neurons, cIPN neurons exhibited a significantly higher  
231 input resistance and a different current-voltage relationship (Figure 5B, S7B) indicating  
232 a distinct cIPN sub-type that we refer to as “Type C”. In cIPN slices, a sub-population of  
233 Type C neurons responded to light stimulation of DAergic afferents with an increase in  
234 spAP frequency that was attenuated in the presence of SCH39166 (Figure 5C-E). To

235 test the mechanism of light-evoked changes in AP frequency in Type C neurons, we  
236 examined excitatory input, recording spEPSCs in response to light. Blue light failed to  
237 evoke a change in either spEPSC frequency or amplitude, suggesting the effect of DA  
238 on spAP frequency in this sub-population was due to post-synaptic D1 receptor  
239 expression (Figure 5F-H). Moreover, we also observed a population of Type C neurons  
240 that exhibited a light-induced decrease in spAP frequency, as well as, a reduction in  
241 spEPSC frequency, that were likewise blocked by SCH39166 (Figure S8D-J). To gain  
242 insight into localization of the DAergic neurons in the VTA that may project to the IPN,  
243 we injected AAV2rg-hSyn-DIO-eGFP into different regions of striatum to label discreet  
244 VTA DAergic neurons in DAT::Cre mice (Figure S8)(43-45). In mice in which paranigral  
245 VTA DAergic neurons were labeled, we could trace projections into the cIPN (Figure  
246 S8A); whereas, in mice in which paranigral neurons were not labeled, DAergic  
247 VTA→IPN projections were less apparent (Figure S8B). Together, these data suggest  
248 that a sub-population of Type C neurons in the cIPN that signal through D1 receptors,  
249 may amplify the VTA DAergic input to other IPN neurons, for instance, vIPN Type A and  
250 Type B neurons, and modulate their responses.

251 **cIPN Type C neurons project to the vIPN to control activity of Type A and Type B**  
252 **neurons.**

253 To test if D1-positive neurons in the cIPN project directly to the vIPN, we expressed  
254 Cre-dependent ChR2-eYFP in the IPN of mice that express Cre under the control of the  
255 DRD1 promoter (DRD1a::Cre mice) via AAV2-mediated gene delivery (Figure 6A).  
256 eYFP signal was observed in cIPN neuronal soma and projections along the

257 cIPN→vIPN plane (Figure 6B). Stimulation of Type C terminals in the vIPN (20Hz, 2 ms  
258 pulse width) resulted in a significant increase of spEPSC frequency in Type A neurons  
259 and a significant decrease of spEPSC frequency in Type B neurons (Figure 6C, D, F,  
260 G). These responses phenocopied the result of bath application of DA in 80% of vIPN  
261 neurons as predicted by their input resistances (compare with Figure 4D-I).  
262 Experiments were repeated in the presence of 1  $\mu$ M TTX and 100  $\mu$ M 4-AP to block  
263 action potentials, and thus, block multi-synaptic responses(32). The changes in EPSC  
264 frequency upon light stimulation were maintained in both Type A and B neurons  
265 suggesting the D1 receptor-expressing Type C cIPN neurons project monosynaptically  
266 to the vIPN (Figure 6E, H). In addition, combined GABA<sub>A</sub> and GABA<sub>B</sub> antagonists  
267 saclofen (10  $\mu$ M) and bicuculline (20  $\mu$ M) blocked the light-evoked change in spEPSC  
268 frequency in both Type A and B vIPN neurons suggesting Type C neurons release  
269 GABA to modulate excitatory synapses in the vIPN (Figure 6I, J). As Type A and B  
270 neurons are morphologically distinct and receive differential innervation from mHb  
271 terminals (see Supplemental Results and Figure S9), which strongly innervate Type A  
272 but not Type B neurons, and mHb terminals in the IPN are known to uniquely increase  
273 excitatory transmission in response to activation of GABA<sub>B</sub> receptors(11,46,47), these  
274 data suggest GABA bidirectionally modulates excitatory synapses on Type A and B  
275 neurons through mHb and non-mHb excitatory inputs, respectively.

276 **Pharmacological manipulation of D1 receptors in the IPN bidirectionally**  
277 **modulates anxiety-like behavior.**

278 To test if D1 signaling in the IPN modulates anxiety-like behavior, we implanted drug  
279 infusion cannulas and delivered a D1 receptor agonist or antagonist into the IPN prior to  
280 testing in the EPM and OFT assays (Figure 7). In the EPM and the OFT, intra-IPN  
281 infusion of the D1 receptor agonist SKF82958 increased open arm time and increased  
282 time in the center, respectively, compared to vehicle infusion, indicating an anxiolytic  
283 effect of the drug. Conversely, the D1 receptor antagonist SCH39166 was anxiogenic,  
284 reducing open arm time and time in the center compared to vehicle infusion (Figure 7B,  
285 D). Neither drug affected the number of arm entries in the EPM, or total distance  
286 traveled in the OFT (Figure 7C, E). Infusion of the D1-like receptor agonist and  
287 antagonist directly into the VTA had little effect on anxiety-like behavior (Figure  
288 S10B,D). However, VTA infusion of D1 drugs resulted in a depression of total arm  
289 entries in the EPM (Figure S10C). The difference in locomotor effects and the lack of a  
290 significant effect on anxiety-like behavior when the VTA was infused suggests behaviors  
291 elicited from IPN infusions were not the result of off target effects from drug diffusion.  
292 Overall, these results demonstrate that endogenous DA controls anxiety-like behavior  
293 via anxiolytic D1 receptor signaling in the IPN.

294

## 295 **Discussion**

296 DA signaling has long been implicated in anxiety-like behavior presumably through  
297 midbrain DA projection areas to the hippocampus, extended amygdala, and prefrontal  
298 cortex, among other brain regions(4-6,34-36). Our data combining GRAB<sub>DA</sub> sensor  
299 expression in the IPN with pharmacology and imaging revealed that endogenous DA is

300 released in the IPN.. Preventing IPN DA increases in vivo by silencing the VTA→IPN  
301 input reduced both exploration of the EPM open arm and exploration of the center of the  
302 OFT. Conversely, activating the input increased time spent in the EPM open arm and  
303 exploration of the center of the OFT, suggesting that this IPN DA signal controls  
304 anxiety-like behavior specifically by driving anxiolysis. Assays used to evaluate anxiety-  
305 like behavior in mice including the EPM and OFT are multimodal and integrate two  
306 opposite motivational drives: 1) behavioral avoidance and 2) novelty seeking(29).  
307 Mice will be driven to explore the open arms of the EPM or center of the OFT because  
308 they are novel but also avoid exploration because they are elevated or open and without  
309 protection from predation. Thus, the read-out or expression of anxiety-like behavior  
310 relies upon the strength of these two motivational drives. Interestingly, previous studies  
311 implicate the habenulo-interpeduncular pathway in behavioral avoidance and  
312 aversion(10,16,19); whereas, we have also discovered that the IPN and associated  
313 circuitry is also critically involved in signaling familiarity, reducing motivation to explore  
314 novelty to control novelty preference(22). Our data indicate that VTA input and IPN DA  
315 may provide a signal that either reduces avoidance behavior to allow expression of  
316 reduced anxiety-like behavior or increase motivation to explore novelty. Future studies  
317 will focus on how the IPN integrates anxiety and novelty signals to drive exploratory  
318 behavior.

319 Activation of DAergic IPN inputs stimulates a small sub-population of dopaminoceptive  
320 neurons expressing the D1 receptor located predominantly in the caudal portion of the  
321 IPN. Through retrograde tracing, our data suggest that a sub-population of accumbens  
322 shell-projecting VTA DA neurons in the paranigral region may preferentially project into

323 the IPN to innervate cIPN neurons, although we cannot rule out that DAergic neurons in  
324 other regions of the VTA, or other brain areas, also may contribute to this circuit, an  
325 issue that will require further experimentation.

326 Remarkably, cIPN neurons, through a microcircuit spanning the vIPN, amplify the DA  
327 signal ultimately controlling anxiety-like behavior. Indeed, the vast majority of vIPN  
328 neurons respond to exogenous DA in midbrain slices (35 out of 39) presumably through  
329 D1 receptor-expressing Type C terminals which modulate excitatory input to vIPN  
330 neurons. One potential caveat with our results is that we used a D1 antagonist, SCH  
331 39166, to block DA effects in midbrain slices. While SCH 39166 is selective for D1/D5  
332 receptors, it can also block D2-like receptors at higher concentrations and may also be  
333 a low affinity antagonist at 5HT2 receptors(48). However, the concentration used in our  
334 experiments was similar to that of other studies examining D1-receptor mediated  
335 responses in rodent brain slices(49-51) and effects of DA signaling we observed in the  
336 IPN persisted in the presence of a D2 antagonist. In addition, the D1 antagonist not  
337 only blocked effects of bath application of DA, but also responses observed by specific  
338 optic activation of VTA DAergic terminals in the IPN. The effect of exogenous DA  
339 application on vIPN neuronal activity was phenocopied by direct optogenetic activation  
340 of D1-expressing terminals in vIPN, supporting a DA signal-amplifying micro-circuit.  
341 Thus, what at first glance would appear to be a modest connection between VTA and  
342 cIPN, through this amplification step, transmits activity to the majority of neurons in the  
343 ventral portion of the nucleus to control behavior.

344 The microcircuit controlling activity of vIPN neurons is unique in that it consists of two  
345 morphologically distinct neurons, Type A and Type B, which both receive GABAergic

346 innervation from cIPN Type C neurons but act oppositely in response to GABA. Type A  
347 neurons are excited by activation of Type C terminals via increased glutamate release;  
348 whereas Type B neurons are inhibited by activation of Type C terminals via decreased  
349 glutamate release (Figure 8). Interestingly, Type A neurons are robustly controlled by  
350 mHb excitatory inputs that are activated by GABA via excitatory GABA<sub>B</sub> receptors on  
351 mHb terminals(11,33). Type B neurons, on the other hand, are weakly innervated by  
352 the mHb, thus, it is likely that GABA reduces excitatory input from other, unidentified  
353 excitatory afferents that express inhibitory GABA receptors. In the future, it will be  
354 necessary to apply additional circuit mapping approaches to identify this excitatory IPN  
355 input. Ultimately, engaging this microcircuit either through optogenetic stimulation of  
356 VTA→IPN inputs or through infusion of D1 receptor agonist increases Type A neuronal  
357 activity while decreasing Type B neuronal activity to reduce anxiety-like behavior.

358 In summary, our data indicate that VTA DAergic input to the IPN mediates anxiety-like  
359 behavior by activating D1-expressing neurons in the cIPN. This small population of  
360 dopaminoceptive neurons amplify VTA DA input by projecting to and innervating vIPN  
361 through mHb glutamatergic inputs to bidirectionally control anxiolysis. Thus, we have  
362 identified a critical component of the neural network contributing to affective state  
363 through DAergic signaling that engages a unique IPN microcircuit.

#### 364 **Author Contributions**

365 S.R.D., R.Z., L.C., P.M.K., and S.M. conducted the experiments. Y.L. provided the  
366 GRAB<sub>DA</sub> sensors. S.R.D., R.Z., L.C., P.M.K., F.S., P.D.G. Y.L. and A.R.T. designed the  
367 experiments. S.R.D. and A.R.T. wrote the paper with input from all co-authors.

## 368 **Acknowledgments**

369 We thank Karl Deisseroth for optogenetic plasmids and Guangping Gao for viral  
370 plasmid packaging. We also thank Anthony Sacino for technical support and Haley  
371 Melikian for insightful discussion. This work was supported by the National Institute on  
372 Drug Abuse award number DA041482 (A.R.T.), DA047678 (A.R.T.), DA035371 (P.D.G.  
373 and A.R.T.), by a NARSAD Independent Investigator Grant from the Brain & Behavior  
374 Research Foundation (A.R.T.), and by the Brudnick Fellowship in Mood Disorders  
375 (P.M.K.). The content is solely the responsibility of the authors and does not necessarily  
376 represent the official views of the National Institutes of Health.

## 377 **Declaration of Interests**

378 The authors report no biomedical financial interests or potential conflicts of interest.

## 379 **Data Availability**

380 The data presented in this study are available from the corresponding author upon  
381 reasonable request.

382

383

## 384 **Figure Legends**

385 **Figure 1. Dopamine sensing in the IPN. (A)** Left, experimental strategy for functional  
386 verification of GRAB<sub>DA2m</sub> in midbrain slices. Middle, heat map of IPN GRAB<sub>DA2m</sub>

387 responses to 2 min bath application of neurotransmitter, applied at t=2 min. Right,  
388 summed average of maximal responses of bath application of neurotransmitter (One  
389 way ANOVA:  $F_{(5, 31)} = 89.6$ ,  $p = 0.0001$ ; Bonferroni's multiple comparisons test:  
390 \*\*\*\* $p < 0.0001$ ). **(B)** Top, heat map of IPN GRAB<sub>DA2m</sub> responses to ACSF (n=10),  
391 amphetamine (AMPH, n=16), or AMPH following pre-application of haloperidol (HALO,  
392 n=6). AMPH applied at t=10 min until the end of recording. Bottom, summed average of  
393 maximal responses from top panel (One way ANOVA:  $F_{(2, 29)} = 35.2$ ,  $p = 0.0001$ ;  
394 Bonferroni's multiple comparisons test: \*\*\*\* $p < 0.0001$ ). **(C)** Top, heat map of IPN  
395 GRAB<sub>DA2m</sub> responses to ACSF (n=6), desipramine (DPA, n=6), AMPH (n=6), or AMPH  
396 following pre-application of DPA (n=6). Bottom, summed average of maximal responses  
397 from top panel (One way ANOVA:  $F_{(3, 20)} = 29.7$ ,  $p = 0.0001$ ; Bonferroni's multiple  
398 comparisons test: \*\*\*\* $p < 0.0001$ ).

399

400 **Figure 2. VTA→IPN DA input controls anxiety-like behavior. (A)** Diagram of strategy  
401 for halorhodopsin experiments. **(B)** Open arm time (left) and total arm entries (right)  
402 during *in vivo* NpHR inhibition of VTA terminals in the IPN of light-on NpHR (n=13) and  
403 light-on eYFP (n=11) DAT<sup>Cre</sup> animals. (Unpaired two-tailed t-test:  $p=0.0006$ . Mean  $\pm$   
404 SEM.) **(C)** OFT activity during *in vivo* NpHR inhibition of VTA terminals in the IPN.  
405 Representative heat map of mouse position (top). Graphs of center time (bottom left)  
406 and total distance traveled (in cm, bottom right, n=11, 14, eYFP and NpHR,  
407 respectively, Unpaired t-test with Welch's correction:  $p=0.023$ . Mean  $\pm$  SEM.). See  
408 Figure S2 for canula placement. **(D)** Top, diagram of strategy for channelrhodopsin  
409 experiments (also see Figure S2). **(E)** Open arm time (left) and total arm entries (right)

410 during *in vivo* 15 Hz stimulation of ChR2-expressing VTA terminals in the IPN for light-  
411 on eYFP (n=10) and light-on ChR2 (n=10) groups. (Unpaired t-test:  $p=0.0038$ . Mean  $\pm$   
412 SEM.) **(F)** OFT activity during *in vivo* 15 Hz stimulation of ChR2-expressing VTA  
413 terminals in the IPN. Representative heat map of mouse position (top). Graphs of center  
414 time (bottom left) and total distance traveled (bottom right). See Figure S2 for canula  
415 placement. (n=12, 10 eYFP and NpHR, respectively, Unpaired t-test:  $p=0.0028$ . Mean  $\pm$   
416 SEM.)

417 **Figure 3. DA modulates neuronal activity in two vIPN neuron sub-populations.**

418 **(A)** Representative cell-attached trace from a Type A neuron in response to DA and **(B)**  
419 AP frequency of Type A neurons at baseline, during the last minute of DA application,  
420 and after washout (Friedman test: Friedman statistic<sub>(2, 34)</sub> = 19.13,  $p<0.0001$ . \*\*\* $p<0.0001$   
421 compared to baseline, Dunn's multiple comparison test. Mean  $\pm$  SEM.). **(C)** Time  
422 course of drug application in Type A neurons. **(D)** Representative cell-attached trace of  
423 a Type B neuron (top) in response to DA and **(E)** AP frequency of Type B neurons at  
424 baseline, during the last minute of DA application, and after washout (Friedman  
425 statistic<sub>(2, 32)</sub> = 22.81,  $p\leq 0.0001$ . \*\*\*\* $p<0.0001$  compared to baseline, Dunn's multiple  
426 comparison test. Mean  $\pm$  SEM.) **(F)** Time course of drug application in Type B neurons.  
427 **(G)** Diagram of a coronal section of the IPN with approximate locations of Type A  
428 neurons (blue circles) and Type B neurons (red circles). Neurons without a response to  
429 DA are depicted as green circles. Location taken from digital images of the recording  
430 pipette in the slice after each recording. Representative traces of Type A **(H)** and B **(I)**  
431 current-voltage relationships in response to 20 pA current injection steps. Traces are to  
432 scale with each other. **(J)** Input resistance of Type A and B neurons calculated from the

433 0 to -20 pA step from traces in (D) and (E). (n = 10 and 12, respectively, unpaired t-test  
 434 with Welch's correction: \*\*\*p=0.0003. Data presented as mean  $\pm$  SEM.) **(K)** Current  
 435 voltage relationship. (Two-way ANOVA: Significant cell-type x current step interaction,  
 436  $F_{(10, 218)}=5.07$ ,  $p = 0.0001$ . Bonferroni's multiple comparisons test: \*\*p $\leq$ 0.01, \*\*\*p $\leq$ 0.001,  
 437 \*\*\*\*p $\leq$ 0.0001. Mean  $\pm$  SEM.)

438 **Figure 4. vIPN neurons respond to DA through presynaptic D1-like but not D2-like**  
 439 **DA receptors. (A)** Schematic of experiment. Dotted lines indicate approximate  
 440 positions where coronal slice was cut (left). Neurons were recorded from a coronal slice  
 441 of the vIPN (right). **(B)** Averaged normalized spAP frequency of Type A neurons in  
 442 response to DA in the absence and presence of the D1-like receptor antagonist  
 443 SCH39166 (10  $\mu$ M, top) or the D2-like receptor antagonist Eticlopride (10  $\mu$ M, bottom).  
 444 (n=6, One-way ANOVAs: (Top)  $F_{(2, 10)} = 19.6$ ,  $p=0.0003$ ; SCH39166:  $F_{(2, 10)} = 0.1435$ ,  
 445  $p=0.8680$ ; (Bottom)  $F_{(2, 10)} = 6.492$ ,  $p=0.016$ ; Eticlopride:  $F_{(2, 10)} = 9.23$ ,  $p=0.0054$ . Data  
 446 presented as mean  $\pm$  SEM.) \*p<0.05, \*\*p<0.01, \*\*\*p<0.001 compared to baseline. **(C)**  
 447 Averaged normalized spAP frequency of Type B neurons in response to DA in the  
 448 absence and presence of the D1-like receptor antagonist SCH39166 (10  $\mu$ M, top) or the  
 449 D2-like receptor antagonist eticlopride (10  $\mu$ M, bottom, n=6, One-way ANOVAs: (Top)  
 450  $F_{(2, 12)} = 8.593$ ,  $p=0.0048$ ; SCH39166:  $F_{(2, 12)} = 1.852$ ,  $p=0.1991$ ; (Bottom)  $F_{(2, 10)} = 17.86$ ,  
 451  $p=0.0005$ ;  $F_{(2, 10)} = 25.79$ ,  $p=0.0001$ ). \*\*p<0.01, \*\*\*p<0.001 compared to baseline, Mean  
 452  $\pm$  SEM. **(D)** Representative whole-cell patch clamp traces of spEPSCs in a Type A  
 453 neuron before, during, and after DA application. **(E)** Type A spEPSC frequency at  
 454 baseline, during last minute of DA application, and after washout (n=10, Friedman test:  
 455 \*\*p $\leq$ 0.01, Friedman statistic $_{(2, 18)} = 9.6$ .,  $p=0.0075$ ). \*\* p<0.01 Dunn's test compared to

456 baseline. Data are mean  $\pm$  SEM. **(F)** Type A spEPSC amplitude at baseline, during last  
457 minute of DA application, and after washout. (n=10, One-way ANOVA:  $F_{(2, 18)} = 0.3592$ ,  
458  $p=0.7031$ ). Data are mean  $\pm$  SEM. **(G)** Representative whole-cell patch clamp traces of  
459 spEPSCs in a Type B neuron before, during, and after DA application. **(H)** Type B  
460 spEPSC frequency at baseline, during last minute of DA application, and after washout  
461 (n=7, One-way ANOVA:  $F_{(2, 12)} = 14.47$ ,  $p=0.0008$ ). \* $p < 0.05$  compared to baseline.  
462 Data are mean  $\pm$  SEM. **(I)** Type A spEPSC amplitude at baseline, during last minute of  
463 DA application, and after washout (One-way ANOVA:  $F_{(2, 12)} = 0.6047$ ,  $p=0.5621$ . Data  
464 are mean  $\pm$  SEM).

465 **Figure 5. Optogenetic stimulation of VTA→IPN DAergic terminals modulate cIPN**  
466 **neurons via D1 receptors. (A)** Schematic of experiment. Cre-dependent ChR2-eYFP  
467 was expressed in putative DAergic neurons of the VTA in DAT<sup>Cre</sup> mice via AAV2-  
468 mediated gene delivery (left). Neurons in the cIPN were recorded in coronal slices while  
469 optogenetically stimulating the DRD1 expressing terminals (right). **(B)** Representative  
470 whole-cell current-clamp traces from a cIPN neuron in response to 20 pA current  
471 injection steps from +100 to -40 pA. Compare to Figure 2A and B. **(C)** Representative  
472 traces of a cIPN neuron that responded to VTA terminal stimulation with an increase in  
473 firing rate. **(D)** spAP frequency of Type C neurons that responded to light stimulation  
474 with an increase in spAP frequency (n=10, One-way ANOVA:  $F_{(2, 18)} = 5.59$ ,  $p=0.013$ ).  
475 \* $p < 0.05$  compared to Light-off control. Data presented as mean  $\pm$  SEM. **(E)** spAP  
476 frequency of cIPN neurons from (D) during 10  $\mu$ M SCH39166 application (Friedman  
477 statistic<sub>(2, 16)</sub> = 5.35,  $p=0.07$ ). Data presented as mean  $\pm$  SEM. **(F)** Representative trace  
478 of EPSC frequency from a cIPN neuron that increased its spAP frequency in response

479 to VTA terminal stimulation. **(G)** In cIPN neurons that increased their spAPs, spEPSC  
480 frequency was not significantly affected. (One-way ANOVA:  $F_{(2, 10)} = 0.1732$ ,  $p=0.8435$ ).  
481 Data presented as mean  $\pm$  SEM. **(H)** In cIPN neurons that increased their spAPs,  
482 spEPSC amplitude was not significantly affected. (One-way ANOVA:  $F_{(2, 10)} = 2.106$ ,  
483  $p=0.1725$ ). Data presented as mean  $\pm$  SEM.

484 **Figure 6. cIPN Type C putative D1 receptor-expressing neurons project to the**  
485 **vIPN and modulate Type A and Type B neuronal activity via GABA. (A)** Schematic  
486 of experiment. Cre-dependent ChR2-eYFP was expressed in putative DRD1-expressing  
487 neurons of the cIPN in DRD1::Cre mice via AAV2-mediated gene delivery (left).  
488 Neurons in the vIPN were recorded in coronal slices while optogenetically stimulating  
489 the DRD1 expressing terminals (right). **(B)** Sagittal slice showing Cre-dependent eYFP  
490 (green) from a (DRD1)::Cre mouse. cIPN neurons send projections rostrally to the vIPN.  
491 **(C)** Representative whole-cell patch clamp traces of Type A neuron EPSCs before,  
492 during and after 20 Hz stimulation of cIPN terminals in the presence of TTX and 4-AP.  
493 **(D)** Type A EPSC response to 20 Hz terminal stimulation. ( $n=8$ , One-way ANOVA:  $F_{(2,$   
494  $14)} = 20.8$ ,  $p=0.0001$ ). \*\*\* $p<0.001$  compared to Light-off control. Data presented as  
495 mean  $\pm$  SEM. **(E)** Type A response to DRD1-Cre terminal stimulation in the presence of  
496 AP blockers. The response was “monosynaptic” ( $n=14$ , Friedman test: Friedman  
497 statistic $_{(2,26)} = 24.57$ ,  $p<0.0001$ ). \*\* $p<0.01$  compared to Light-off control. Data presented  
498 as mean  $\pm$  SEM. **(F)** Representative whole-cell patch clamp traces of Type B neuron  
499 EPSCs before, during and after stimulation of cIPN terminals in the presence of TTX  
500 and 4-AP. **(G)** Type B response to 20 Hz terminal stimulation ( $n=7$ , One-way ANOVA:  $F_{(2,$   
501  $12)} = 4.4$ ,  $p=0.037$ ). \* $p<0.05$  compared to Light-off control. Data presented as mean  $\pm$

502 SEM. **(H)** Type B response to 20 Hz DRD1-Cre terminal stimulation in the presence of  
503 AP blockers. The connection was monosynaptic (n=9, One-way ANOVA:  $F_{(2, 16)} = 6.58$ ,  
504  $p=0.0082$ ). \*\* $p<0.01$  compared to Light-off control. Data presented as mean  $\pm$  SEM. **(I)**  
505 Normalized EPSC frequency of a Type A neuron before, during, and after cIPN DRD1-  
506 Cre terminal stimulation in the presence of 1  $\mu$ M TTX and 100  $\mu$ M 4-AP. The  
507 experiment was repeated with the addition of bath-applied 20  $\mu$ M Bicuculline and 100  
508  $\mu$ M Saclofen to block GABA<sub>A</sub> and GABA<sub>B</sub> receptors, respectively. (n=7, One-way  
509 ANOVAs:  $F_{(2, 12)} = 10.08$ ,  $p=0.0027$ ; GABA<sub>A+B</sub> receptor antagonists:  $F_{(2, 12)} = 1.539$ ,  $p=$   
510  $0.2542$ ). \*\* $p<0.01$  compared to Light-off control. Data are presented as mean  $\pm$  SEM.  
511 **(J)** Normalized EPSC frequency of a Type B neuron before, during, and after cIPN  
512 DRD1-Cre terminal stimulation in the presence of 1  $\mu$ M TTX and 100  $\mu$ M 4-AP. The  
513 experiment was repeated with the addition of bath-applied 20  $\mu$ M Bicuculline and 100  
514  $\mu$ M Saclofen to block GABA<sub>A</sub> and GABA<sub>B</sub> receptors, respectively. (n=5, One-way  
515 ANOVA:  $F_{(2, 8)} = 7.437$ ,  $p=0.015$ ; GABA<sub>A+B</sub> receptor antagonists:  $F_{(2, 8)} = 3.458$ ,  $p=$   
516  $0.0827$ ). \* $p<0.05$  compared to Light-off control. Data are presented as mean  $\pm$  SEM.

517

518 **Figure 7. Manipulation of D1 receptors in the IPN controls anxiety-like behaviors.**

519 **(A)** Diagram of experiment (left). Representative image of guide canula track in slice  
520 immune-labeled with TH antibody (green, also see Figure S11F). **(B)** Quantification of  
521 open arm time in the EPM between D1-like DA receptor agonist (n=10, SKF82598 0.7  
522  $\mu$ g/ $\mu$ l, infused 0.3  $\mu$ l, 210 ng), antagonist (n=13, SCH39166 35 ng/ $\mu$ l, infused 0.3  $\mu$ l,  
523 10.5 ng), or saline control (n=15). (One-way ANOVA with repeated measures:  $F_{(2, 35)}=$

524 11.43,  $p = 0.0002$ ).  $*p \leq 0.05$ ,  $***p \leq 0.001$ . Data presented as mean  $\pm$  SEM. **(C)** Total arm  
525 entries in the EPM after drug infusion. (One-way ANOVA with repeated measures:  $F_{(2, 35)} = 0.6541$ ,  $p=0.5261$ ). Data presented as mean  $\pm$  SEM. **(D)** Representative heat map  
526 of mouse position in the OFT after infusion of drug into the IPN (left). Quantification of  
527 center time in the OFT (right). ( $n=10, 9, 8$  for saline, agonist, antagonist, respectively,  
528 One-way ANOVA with repeated measures:  $*p \leq 0.05$ ,  $**p \leq 0.01$ ,  $F_{(2, 24)} = 8.558$ . Mean  $\pm$   
529 SEM.) **(E)** Quantification of total distance moved in the OFT. There was no significant  
530 difference between groups. (One-way ANOVA with repeated measures:  $F_{(2, 24)} = 1.437$ ,  
531  $p=0.2574$ ). Data are presented as mean  $\pm$  SEM.

533 **Figure 8. Circuit model for DA signal amplification in the IPN.** Circles represent  
534 neurons, the lines originating from the circles represent axons and the triangles  
535 represent terminals. The terminals are set so that the side of the triangle opposite the  
536 axon faces its presumed target. Each color represents a unique population of neurons.

537

538

539

540

541

542

543

544

545

546

547

548

549

550 **References**

- 551 1 Lieb, R. Anxiety disorders: clinical presentation and epidemiology. *Handb Exp*  
552 *Pharmacol*, 405-432 (2005).
- 553 2 Chisholm, D., Sweeny, K., Sheehan, P., Rasmussen, B., Smit, F., Cuijpers, P. *et al.*  
554 Scaling-up treatment of depression and anxiety: a global return on investment analysis.  
555 *The lancet. Psychiatry* **3**, 415-424, doi:10.1016/S2215-0366(16)30024-4 (2016).
- 556 3 Calhoun, G. G. & Tye, K. M. Resolving the neural circuits of anxiety. *Nat Neurosci* **18**,  
557 1394-1404, doi:10.1038/nn.4101 (2015).
- 558 4 Zweifel, L. S., Fadok, J. P., Argilli, E., Garelick, M. G., Jones, G. L., Dickerson, T. M. *et al.*  
559 *et al.* Activation of dopamine neurons is critical for aversive conditioning and prevention of  
560 generalized anxiety. *Nat Neurosci* **14**, 620-626, doi:10.1038/nn.2808 (2011).
- 561 5 Jennings, J. H., Sparta, D. R., Stamatakis, A. M., Ung, R. L., Pleil, K. E., Kash, T. L. *et al.*  
562 *et al.* Distinct extended amygdala circuits for divergent motivational states. *Nature* **496**,  
563 224-228, doi:10.1038/nature12041 (2013).
- 564 6 Refojo, D., Schweizer, M., Kuehne, C., Ehrenberg, S., Thoeringer, C., Vogl, A. M. *et al.*  
565 *et al.* Glutamatergic and dopaminergic neurons mediate anxiogenic and anxiolytic effects of  
566 CRHR1. *Science* **333**, 1903-1907, doi:science.1202107 [pii]10.1126/science.1202107  
567 (2011).
- 568 7 Berry, A. S., White, R. L., Furman, D. J., Naskolnakorn, J. R., Shah, V. D., D'Esposito,  
569 *et al.* Dopaminergic mechanisms underlying normal variation in trait anxiety. *J*  
570 *Neurosci*, doi:10.1523/JNEUROSCI.2382-18.2019 (2019).
- 571 8 Jesuthasan, S. Fear, anxiety and control in the zebrafish. *Dev Neurobiol*,  
572 doi:10.1002/dneu.20873 (2011).
- 573 9 Okamoto, H. & Aizawa, H. Fear and anxiety regulation by conserved affective circuits.  
574 *Neuron* **78**, 411-413, doi:10.1016/j.neuron.2013.04.031 (2013).
- 575 10 Soria-Gomez, E., Busquets-Garcia, A., Hu, F., Mehidi, A., Cannich, A., Roux, L. *et al.*  
576 *et al.* Habenular CB1 Receptors Control the Expression of Aversive Memories. *Neuron* **88**,  
577 306-313, doi:10.1016/j.neuron.2015.08.035 (2015).
- 578 11 Zhang, J., Tan, L., Ren, Y., Liang, J., Lin, R., Feng, Q. *et al.* Presynaptic Excitation via  
579 GABAB Receptors in Habenula Cholinergic Neurons Regulates Fear Memory  
580 Expression. *Cell* **166**, 716-728, doi:10.1016/j.cell.2016.06.026 (2016).

- 581 12 Molas, S., DeGroot, S. R., Zhao-Shea, R. & Tapper, A. R. Anxiety and Nicotine  
582 Dependence: Emerging Role of the Habenulo-Interpeduncular Axis. *Trends Pharmacol*  
583 *Sci* **38**, 169-180, doi:10.1016/j.tips.2016.11.001 (2017).
- 584 13 Shibata, H., Suzuki, T. & Matsushita, M. Afferent projections to the interpeduncular  
585 nucleus in the rat, as studied by retrograde and anterograde transport of wheat germ  
586 agglutinin conjugated to horseradish peroxidase. *J Comp Neurol* **248**, 272-284,  
587 doi:10.1002/cne.902480210 (1986).
- 588 14 Lima, L. B., Bueno, D., Leite, F., Souza, S., Gonçalves, L., Furigo, I. C. *et al.* Afferent  
589 and efferent connections of the interpeduncular nucleus with special reference to circuits  
590 involving the habenula and raphe nuclei. *J Comp Neurol* **525**, 2411-2442,  
591 doi:10.1002/cne.24217 (2017).
- 592 15 Fowler, C. D., Lu, Q., Johnson, P. M., Marks, M. J. & Kenny, P. J. Habenular alpha5  
593 nicotinic receptor subunit signalling controls nicotine intake. *Nature* **471**, 597-601,  
594 doi:nature09797 [pii]10.1038/nature09797 (2011).
- 595 16 Fowler, C. D. & Kenny, P. J. Nicotine aversion: Neurobiological mechanisms and  
596 relevance to tobacco dependence vulnerability. *Neuropharmacology* **76 Pt B**, 533-544,  
597 doi:10.1016/j.neuropharm.2013.09.008 (2014).
- 598 17 Zhao-Shea, R., Liu, L., Pang, X., Gardner, P. D. & Tapper, A. R. Activation of  
599 GABAergic neurons in the interpeduncular nucleus triggers physical nicotine withdrawal  
600 symptoms. *Curr Biol* **23**, 2327-2335, doi:10.1016/j.cub.2013.09.041 (2013).
- 601 18 Zhao-Shea, R., DeGroot, S. R., Liu, L., Vallaster, M., Pang, X., Su, Q. *et al.* Increased  
602 CRF signalling in a ventral tegmental area-interpeduncular nucleus-medial habenula  
603 circuit induces anxiety during nicotine withdrawal. *Nature communications* **6**, 6770,  
604 doi:10.1038/ncomms7770 (2015).
- 605 19 Wolfman, S. L., Gill, D. F., Bogdanic, F., Long, K., Al-Hasani, R., McCall, J. G. *et al.*  
606 Nicotine aversion is mediated by GABAergic interpeduncular nucleus inputs to  
607 laterodorsal tegmentum. *Nature communications* **9**, 2710, doi:10.1038/s41467-018-  
608 04654-2 (2018).
- 609 20 Yamaguchi, T., Danjo, T., Pastan, I., Hikida, T. & Nakanishi, S. Distinct roles of  
610 segregated transmission of the septo-habenular pathway in anxiety and fear. *Neuron* **78**,  
611 537-544, doi:10.1016/j.neuron.2013.02.035 (2013).
- 612 21 Pang, X. Liu, L., Ngolab, J., Zhao-Shea, R., McIntosh, J. M., Gardner, P. D. *et al.*  
613 Habenula cholinergic neurons regulate anxiety during nicotine withdrawal via nicotinic  
614 acetylcholine receptors. *Neuropharmacology* **107**, 294-304,  
615 doi:10.1016/j.neuropharm.2016.03.039 (2016).
- 616 22 Molas, S., Zhao-Shea, R., Liu, L., DeGroot, S. R., Gardner, P. D., Tapper, A. R. A  
617 circuit-based mechanism underlying familiarity signaling and the preference for novelty.  
618 *Nat Neurosci* **20**, 1260-1268, doi:10.1038/nn.4607 (2017).
- 619 23 Tsai, H. C., Zhang, F., Adamantidis, A., Stuber, G. D., Bonci, A., de Lecea, L. *et al.*  
620 Phasic firing in dopaminergic neurons is sufficient for behavioral conditioning. *Science*  
621 **324**, 1080-1084, doi:1168878 [pii]10.1126/science.1168878 (2009).
- 622 24 Adamantidis, A. R., Adamantidis, A. R., Tsai, H. C., Boutrel, B., Zhang, F., Stuber, G. D.,  
623 Budygin, E. A. *et al.* Optogenetic interrogation of dopaminergic modulation of the  
624 multiple phases of reward-seeking behavior. *J Neurosci* **31**, 10829-10835,  
625 doi:10.1523/JNEUROSCI.2246-11.2011 (2011).
- 626 25 Chaudhury, D., Walsh, J. J., Friedman, A. K., Juarez, B., Ku, S. M., Koo, J. W. *et al.*  
627 Rapid regulation of depression-related behaviours by control of midbrain dopamine  
628 neurons. *Nature* **493**, 532-536, doi:10.1038/nature11713 (2013).

- 629 26 Tye, K. M., Mirzabekov, J. J., Warden, M. R., Ferenczi, E. A., Tsai, H. C., Finkelstein, J.  
630 *et al.* Dopamine neurons modulate neural encoding and expression of depression-  
631 related behaviour. *Nature* **493**, 537-541, doi:10.1038/nature11740 (2013).
- 632 27 Gunaydin, L. A., Grosenick, L., Finkelstein, J. C., Kauvar, I. V., Fenno, L. E., Adhikari, A.  
633 *et al.* Natural neural projection dynamics underlying social behavior. *Cell* **157**, 1535-  
634 1551, doi:10.1016/j.cell.2014.05.017 (2014).
- 635 28 Sun, F., Zeng, J., Jing, M., Zhou, J., Feng, J., Owen, S. F. *et al.* A Genetically Encoded  
636 Fluorescent Sensor Enables Rapid and Specific Detection of Dopamine in Flies, Fish,  
637 and Mice. *Cell* **174**, 481-496 e419, doi:10.1016/j.cell.2018.06.042 (2018).
- 638 29 Walf, A. A. & Frye, C. A. The use of the elevated plus maze as an assay of anxiety-  
639 related behavior in rodents. *Nature protocols* **2**, 322-328, doi:10.1038/nprot.2007.44  
640 (2007).
- 641 30 Gradinaru, V., Zhang, F., Ramakrishnan, C., Mattis, J., Prakash, R., Diester, I. *et al.*  
642 Molecular and cellular approaches for diversifying and extending optogenetics. *Cell* **141**,  
643 154-165, doi:10.1016/j.cell.2010.02.037 (2010).
- 644 31 Ade, K. K., Wan, Y., Chen, M., Gloss, B. & Calakos, N. An Improved BAC Transgenic  
645 Fluorescent Reporter Line for Sensitive and Specific Identification of Striatonigral  
646 Medium Spiny Neurons. *Frontiers in systems neuroscience* **5**, 32,  
647 doi:10.3389/fnsys.2011.00032 (2011).
- 648 32 Petreanu, L., Mao, T., Sternson, S. M. & Svoboda, K. The subcellular organization of  
649 neocortical excitatory connections. *Nature* **457**, 1142-1145, doi:10.1038/nature07709  
650 (2009).
- 651 33 Ren, J., Qin C., Hu, F., Tan, J., Qiu, L., Zhao, S. *et al.* Habenula "cholinergic" neurons  
652 co-release glutamate and acetylcholine and activate postsynaptic neurons via distinct  
653 transmission modes. *Neuron* **69**, 445-452, doi:S0896-6273(10)01088-3  
654 [pii]10.1016/j.neuron.2010.12.038 (2011).
- 655 34 Liu, J., Perez, S. M., Zhang, W., Lodge, D. J. & Lu, X. Y. Selective deletion of the leptin  
656 receptor in dopamine neurons produces anxiogenic-like behavior and increases  
657 dopaminergic activity in amygdala. *Mol Psychiatry* **16**, 1024-1038,  
658 doi:10.1038/mp.2011.36 (2011).
- 659 35 Kim, S. Y., Adhikari, A., Lee, S. Y., Marshel, J. H., Kim, C. K., Mallory, C. S. *et al.*  
660 Diverging neural pathways assemble a behavioural state from separable features in  
661 anxiety. *Nature* **496**, 219-223, doi:10.1038/nature12018 (2013).
- 662 36 Zhong, P., Vickstrom, C. R., Liu, X., Hu, Y., Yu, L., Yu, H. G. *et al.* HCN2 channels in the  
663 ventral tegmental area regulate behavioral responses to chronic stress. *eLife* **7**,  
664 doi:10.7554/eLife.32420 (2018).
- 665 37 Shevtsova, Z., Malik, J. M., Michel, U., Bahr, M. & Kugler, S. Promoters and serotypes:  
666 targeting of adeno-associated virus vectors for gene transfer in the rat central nervous  
667 system in vitro and in vivo. *Exp Physiol* **90**, 53-59 (2005).
- 668 38 Zhao-Shea, R., Liu, L., Soll, L. G., Impropo, M. R., Meyers, E. E., McIntosh, J. M., *et al.*  
669 Nicotine-mediated activation of dopaminergic neurons in distinct regions of the ventral  
670 tegmental area. *Neuropsychopharmacology* **36**, 1021-1032, doi:npp2010240  
671 [pii]10.1038/npp.2010.240 (2011).
- 672 39 Klenowski, P. M., Fogarty, M. J., Belmer, A., Noakes, P. G., Bellingham, M. C., Bartlett,  
673 S. E. Structural and functional characterization of dendritic arbors and GABAergic  
674 synaptic inputs on interneurons and principal cells in the rat basolateral amygdala. *J*  
675 *Neurophysiol* **114**, 942-957, doi:10.1152/jn.00824.2014 (2015).
- 676 40 Sholl, D. A. Dendritic organization in the neurons of the visual and motor cortices of the  
677 cat. *Journal of anatomy* **87**, 387-406 (1953).

- 678 41 Klenowski, P. M. *et al.* Increased Synaptic Excitation and Abnormal Dendritic Structure  
679 of Prefrontal Cortex Layer V Pyramidal Neurons following Prolonged Binge-Like  
680 Consumption of Ethanol. *eNeuro* **3**, doi:10.1523/ENEURO.0248-16.2016 (2016).
- 681 42 Harris, K. M. & Kater, S. B. Dendritic spines: cellular specializations imparting both  
682 stability and flexibility to synaptic function. *Annu Rev Neurosci* **17**, 341-371,  
683 doi:10.1146/annurev.ne.17.030194.002013 (1994).
- 684 43 Beier, K. T., Steinberg, E. E., DeLoach, K. E., Xie, S., Miyamichi, K., Schwarz, L. et al.  
685 Circuit Architecture of VTA Dopamine Neurons Revealed by Systematic 1084 Input-  
686 Output Mapping. *Cell* **162**, 622-634, doi:10.1016/j.cell.2015.07.015 (2015). 1085
- 687 44 Lerner, T. N., Shilyansky, C., Davidson, T. J., Evans, K. E., Beier, K. T., Zalocusky, K. A.  
688 et al. Intact-Brain Analyses Reveal Distinct Information Carried by SNc 1086 Dopamine  
689 Subcircuits. *Cell* **162**, 635-647, doi:10.1016/j.cell.2015.07.014 (2015). 1087
- 690 45 Menegas, W., Akiti, K., Amo, R., Uchida, N. & Watabe-Uchida, M. Dopamine neurons  
691 1088 projecting to the posterior striatum reinforce avoidance of threatening stimuli. *Nat*  
692 *Neurosci* **21**, 1421-1430, doi:10.1038/s41593-018-0222-1 (2018).
- 693 46 Koppensteiner P., Melani R., Ninan I. A cooperative mechanism involving Ca<sup>2+</sup>-  
694 permeable AMPA receptors and retrograde activation of GABAB receptors in interpeduncular  
695 nucleus plasticity. *Cell Rep.* 2017 Aug 1; 20(5): 1111–1122. doi: 10.1016/j.celrep.2017.07.013
- 696 47 Melani R., Von Itter R., Jing D., Koppensteiner P., Ninan I. Opposing effects of an  
697 atypical glycinergic and substance P transmission on interpeduncular nucleus plasticity.  
698 *Neuropsychopharmacology*. 2019 Sep;44(10):1828-1836. doi: 10.1038/s41386-019-0396-6.  
699 Epub 2019 Apr 20.
- 700 48 McQuade R.D., Duffy R.A., Anderson C.C., Crosby G., Coffin V.L., Chipkin R.E., Barnett  
701 A. [<sup>3</sup>H]SCH 39166, a new D1-selective radioligand: in vitro and in vivo binding analyses. *J*  
702 *Neurochem.* 1991 Dec;57(6):2001-10.
- 703 49 Aosaki T., Kiuchi k., Kawaguchi Y. Dopamine D1-Like Receptor Activation Excites Rat  
704 Striatal Large Aspiny Neurons In Vitro. *J Neurosci.* 1998 Jul 15; 18(14): 5180–5190. doi:  
705 10.1523/JNEUROSCI.18-14-05180.1998
- 706 50 Nimitvilai S., Brodie M.S. Reversal of Prolonged Dopamine Inhibition of Dopaminergic  
707 Neurons of the Ventral Tegmental Area. *J Pharmacol Exp Ther.* 2010 May; 333(2): 555-563.  
708 doi: 10.1124/jpet.109.163931
- 709 51 Liu S., Plachez C., Shao Z., Puche A., Shipley M.T. Olfactory Bulb Short Axon Cell  
710 Release of GABA and Dopamine Produces a Temporally Biphasic Inhibition–Excitation  
711 Response in External Tufted Cells. *J Neurosci.* 2013 Feb 13; 33(7): 2916–2926. doi:  
712 10.1523/JNEUROSCI.3607-12.2013

713

714

715

Figure 1

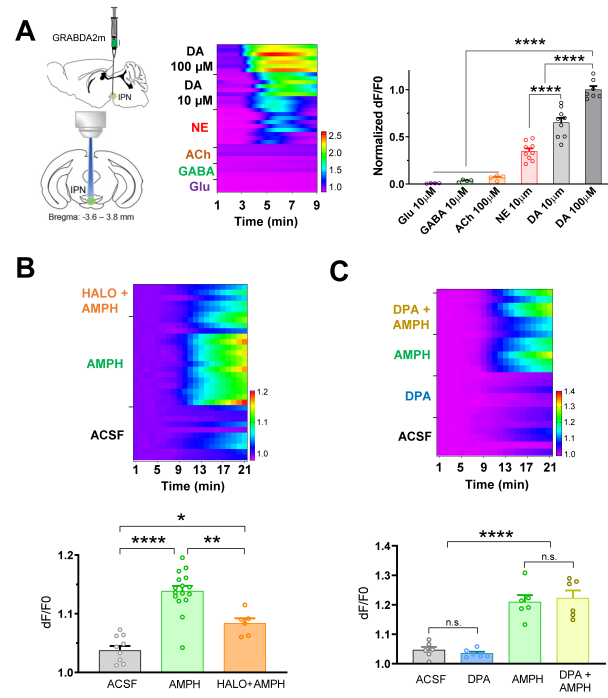


Figure 3.

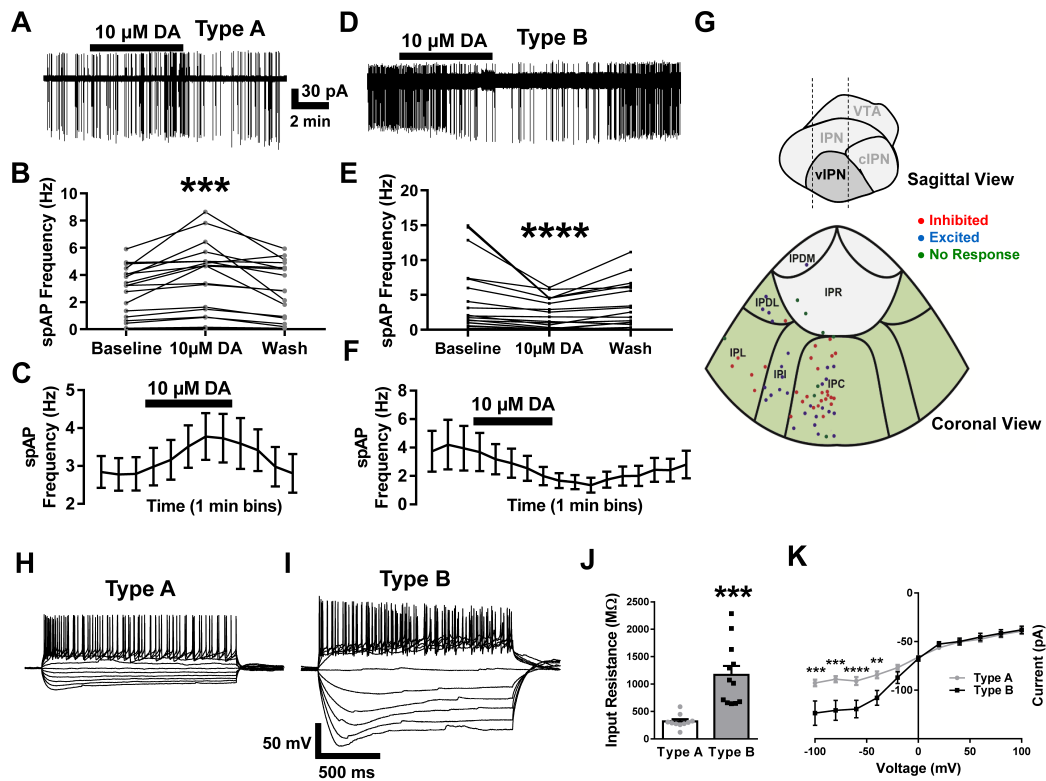


Figure 5.

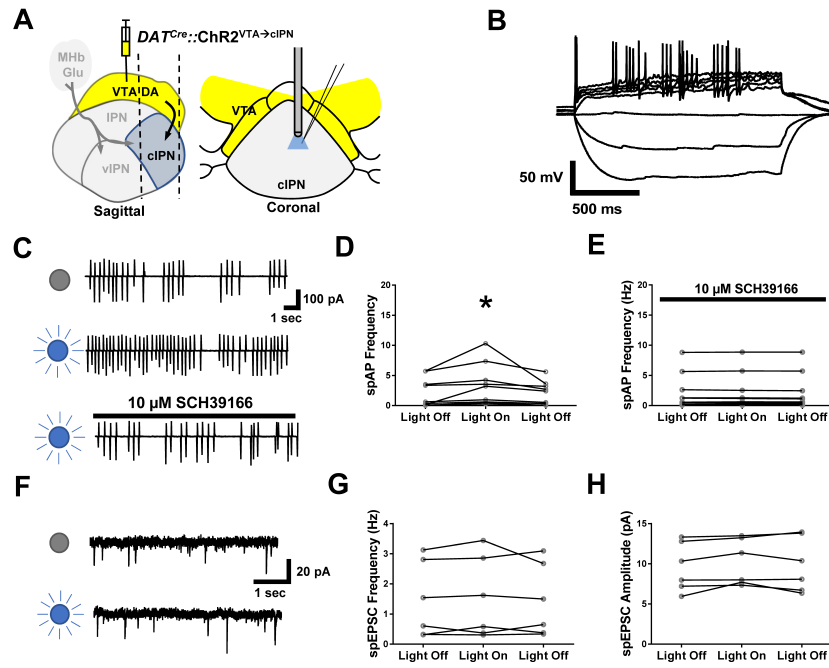


Figure 6.

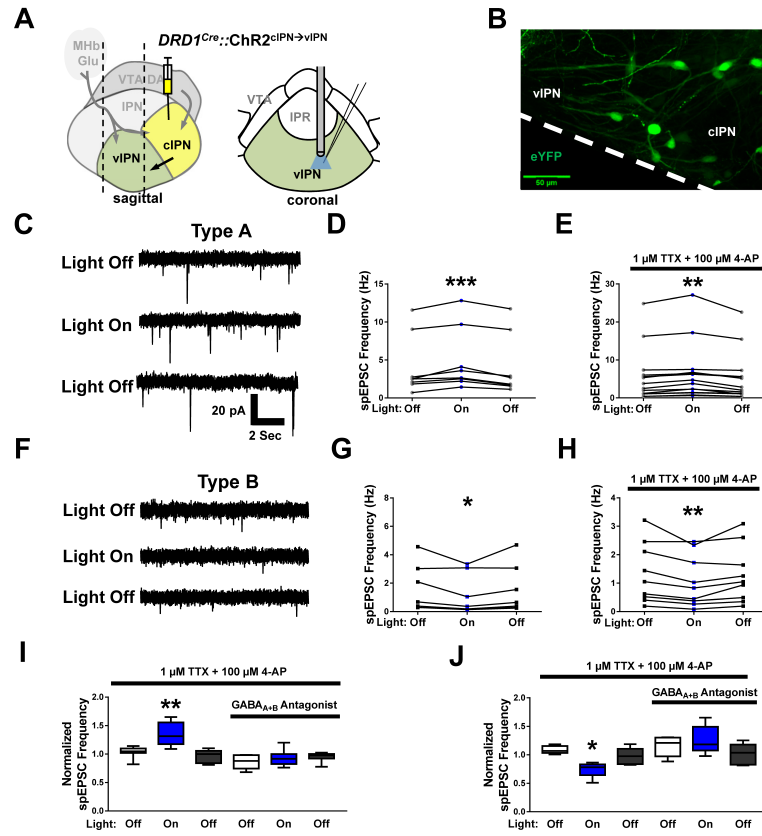


Figure 2

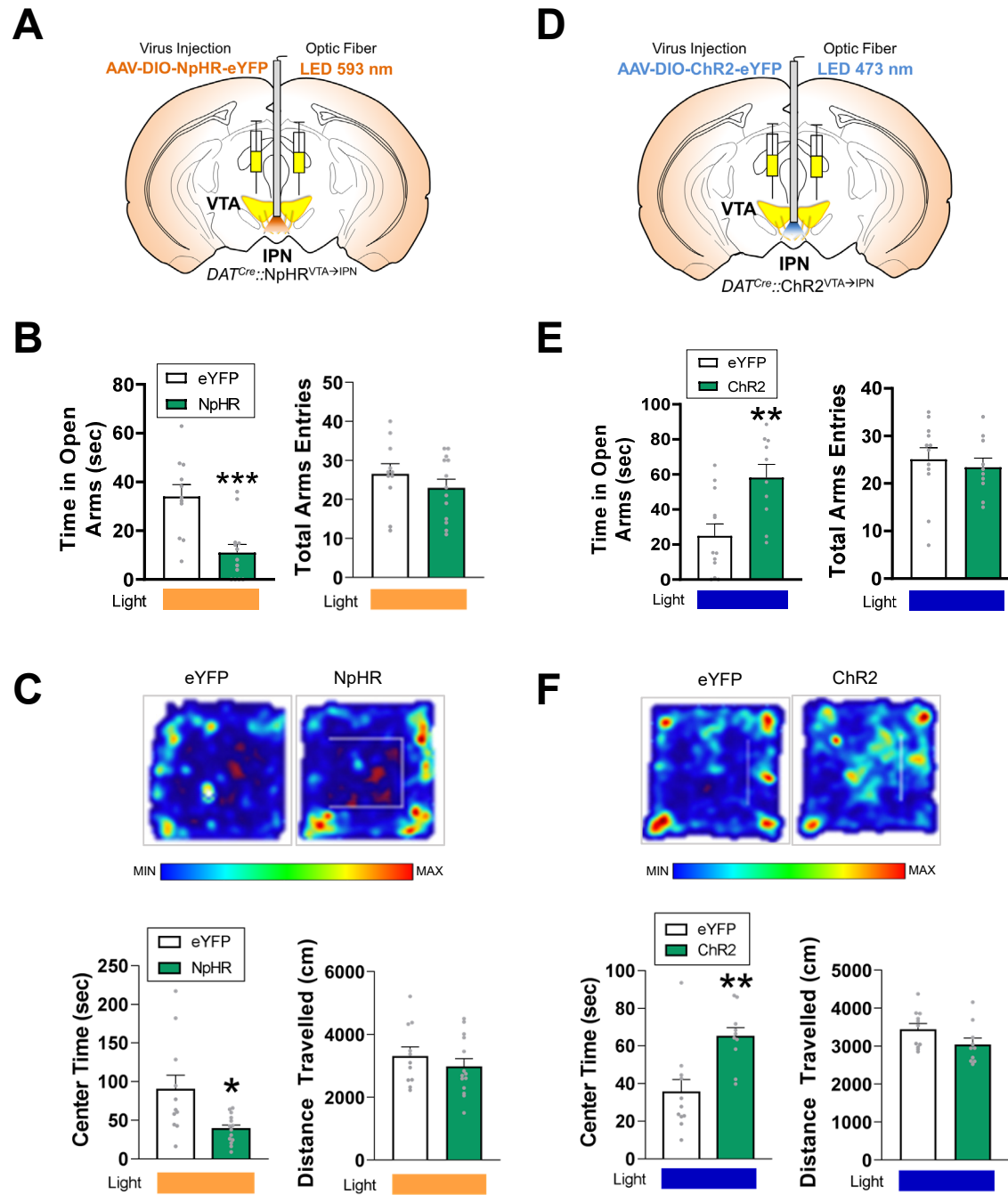


Figure 4.

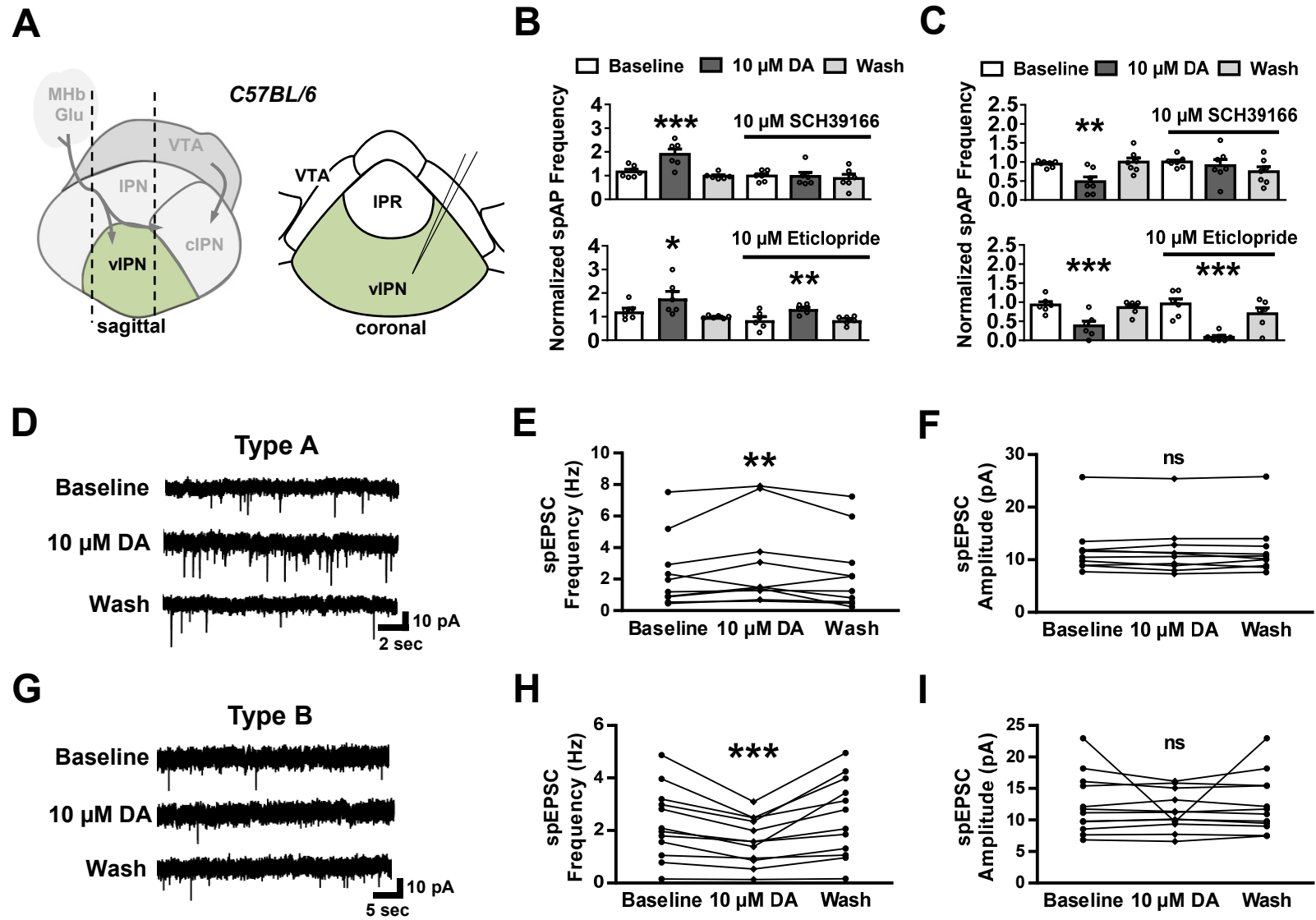


Figure 8.

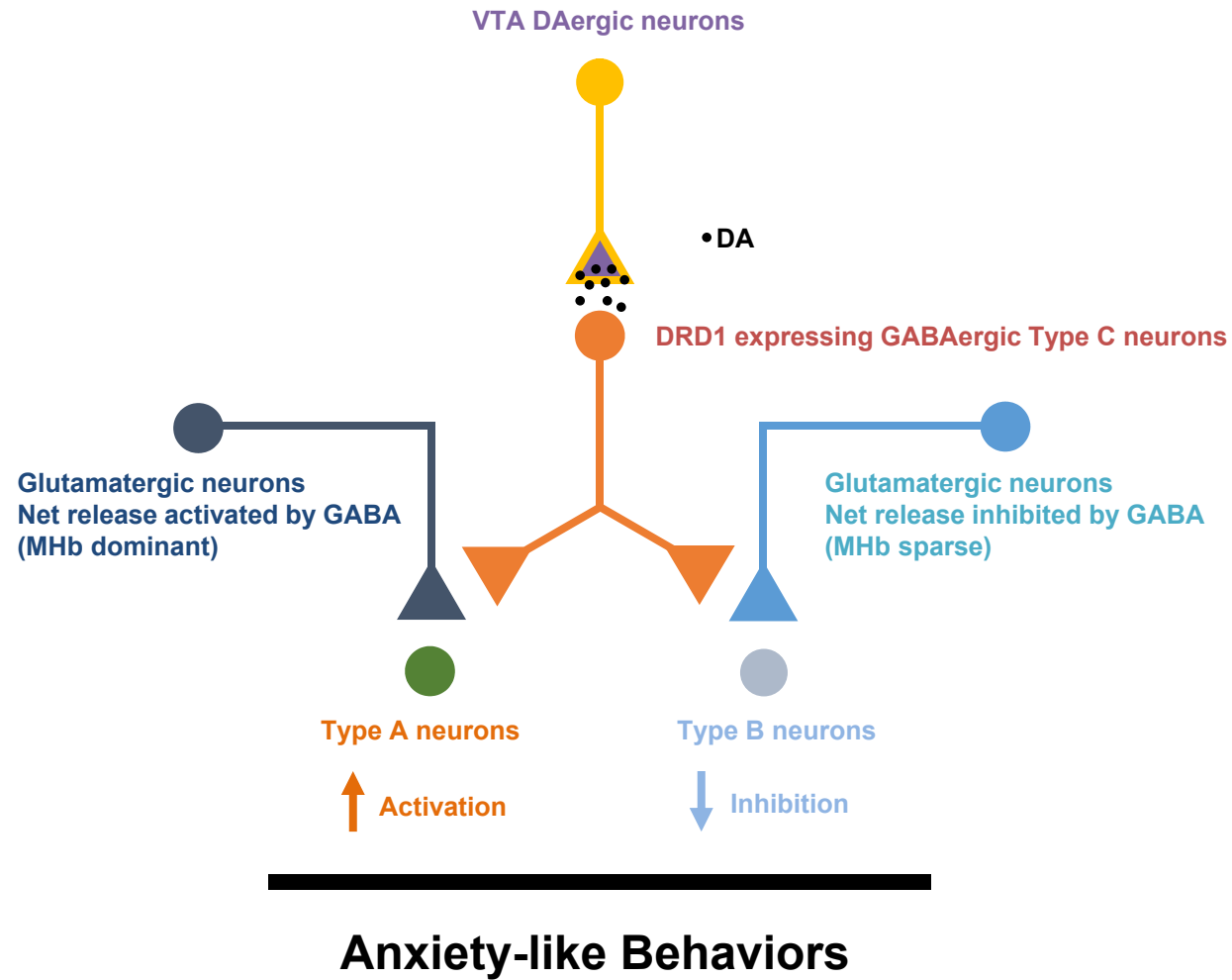


Figure 7

